

# Implementation and Derivation Kinematics Modeling Analysis of WidowX 250 6Degree of Freedom Robotic Arm

Hasan A. Obied<sup>1\*</sup> , Manaf K. H. Al-Taleb<sup>1</sup> , Hind Zuhair Khaleel<sup>2</sup> , Ali F. AbdulKareem<sup>3</sup> 

<sup>1</sup>Electrical Department, College of Engineering, University of Wasit, Wasit, Iraq

<sup>2</sup>Control and Systems Engineering Department, University of Technology, Baghdad, Iraq

<sup>3</sup>Al-Swaira Technical Institute, Middle Technical University, Wasit, Iraq

\*Email: [hassaina302@uowasit.edu.iq](mailto:hassaina302@uowasit.edu.iq)

Article Info	Abstract
<b>Received</b> 09/02/2024 <b>Revised</b> 26/03/2025 <b>Accepted</b> 18/05/2025	<p>Many industries use robotic arms to perform tasks like picking and placing. The main goal of this paper is to derive and implement the forward and inverse kinematics of a 6-degree-of-freedom articulated robotic arm. In addition, a closed-form solution is required to design the inverse kinematics, unlike the forward kinematics. Then, the inverse kinematics and forward kinematics modeling were successfully performed on the WidowX 250 6-degree-of-freedom robotic arm. The MATLAB modeling results are compared to the ROS results, which showed a matching percentage of 99%. In addition, the inverse kinematics results revealed a range of solutions that are approximately identified to the desired results, while others were not, such as the value of the third joint angle is obtained at <math>\pm 1.57</math> radians. Finally, due to the accuracy value of this comparative work between real ROS and MATLAB derived equations of the WidowX 250 6DOF robot arm, it is concluded that the joints and coordinates of this robot are identified.</p>

**Keywords:** End Effector; Forward Kinematics; Inverse Kinematics; Robotic Operation System; WidowX 250

## 1. Introduction

Robotics is a state-of-the-art field of modern technology that crosses traditional engineering boundaries in industrial applications. A comprehensive understanding of robots and their applications requires an education in (mechanical, electrical, systems, and industrial engineering, economics, computer science, and mathematics) [1]. In addition, the robotic arm is referred to as the manipulator, and a redundant manipulator robot is composed of links joined together by joints, similar to a chain. Kinematics problems are represented by manipulator motion without force and torque perception. The robotic arm system was widely used in processing product transportation, production, domestic services, and others because of its advantages such as (high efficiency, precise movements, and capacity for carrying) [2], [3].

In a robotic arm, degrees of freedom are the number of independent variables or directions a robot arm can move. The more degrees of freedom DOF a robot arm has, the more complex movements and tasks it can perform. A robotic arm typically has between 2 and 7 degrees of freedom, depending on its design and intended usage. A 2-DOF robot arm can move in two directions, such as up-down or left-right. A three-degree-

of-freedom robot arm can move in three rotational movements, such as left-right, down-up, and backward-forward [4], [5]. The robotic arms of most industrial robots have six degrees of freedom, which means the robotic arms can move in six different directions, including rotational motion in three axes. This enabled the robotic arm to move more dexterously and flexibly, allowing it to perform multiple tasks such as welding and assembling components. In this paper, the WidowX250 (6 DOF robot arm) was manufactured and designed by Trossen Robotics. The 6-axis robotic arm was built to be precise, highly versatile, and adaptable to various applications [6].

Bao et al. [7] studied the kinematic model of a 4-DOF manipulator, and Robot Toolbox was used to simulate and analyze the forward and inverse kinematics, as well as the trajectory planning for the manipulator for the working space diagram [7]. Chao et al. [8] investigated Cartesian space for a geometrical inverse solution to drive a space and a hydraulic manipulator for four degrees of freedom. The divergent and structural characteristics of the manipulator were analyzed in the FK using the Denavit Hartenberg (DH) technique. Under the kinematics constraint, the manipulator's EE's orientation and position can be determined. The inverse kinematics IK

solutions of the robotic arm can be obtained by analyzing the structure, and the robot's mechanism can determine the communication between joint-space and drive-space. IK and conversion are validated using simulation to meet manipulator motion planning and control needs. The operating and design of a pick and place arm robot was applied in the packaging of tomatoes with a gripper at the EE to grab an object and place it somewhere else, as discussed by Dewi et al. in [9].

Implementing an IK analysis of a 4-DOF arm robot manipulator design with an FLC (fuzzy logic controller) to ensure smooth grab movement does not require much research. The input and experimental results were compared to explain the efficiency of the suggested approach. In [10], the author described the design of the mechanical equations of a 4-DOF robotic manipulator used in industry development. The manipulator's kinematic analysis was developed using IK to determine the precise model that indicated the joint positions. In IK, an optimized computational algorithm was used to obtain the angular joint values without requiring too much algebraic and computational processing. The researcher in [11] analyzed various kinematic modeling approaches that included applicability, difficulty to a certain type of robot, and the required joint variables to define that type of robot. A 5-DOF articulated manipulator was used in a similar investigation to demonstrate how different methods can be applied to obtain the valid parametric method needed to design precise kinematic models. A sensor used in medical applications and robot IK of complex robotic arms was solved for redundancy manipulators using an Adaptive Neuro Fuzzy Inference System (ANFIS), respectively [12], [13].

In 2015, Das and Mahapatra proposed an approach to predict the inverse kinematics of a Pioneer robotic arm with a 6 DOF end-effector using an Adaptive Neuro-Fuzzy Inference System (ANFIS) [14]. Modeling, forward kinematics of a 6-DOF robotic arm from DFROBOT on LabVIEW was presented. Denavit-Hartenberg (DH) representation method was used to determine the forward kinematics, while the inverse kinematics was solved analytically using the geometrical method [15]. In another study, an approach was designed to solve the inverse kinematics problem of a redundant robot manipulator that combines the Neural Network (NN) and Genetic Algorithm (GA) techniques to obtain an optimal solution to the inverse kinematics problem [16]. Other studies addressed the work related to the robotic arm to automatically grasp and classify the target, placing it in a specified area [17]-[20]. Obied et al. studied the visualizing kinematics of altered joint angles on end effector orientation and position for the Widowx250 6DOF robotic arm [21]. As such, based on our previous publications, this paper derives and implements the forward and inverse kinematics of a 6-degree-of-freedom articulated robotic arm. In addition, the current study was conducted to simulate the Trossen Robotics WidowX250 6DOF robotic arm at the University of Wasit.

In this research, the kinematics of the WidowX 250 robotic arm with its DH parameters is explained in section 2, followed by the forward kinematics FK and inverse kinematics (IK analysis methods in section 3. Section 4 illustrates the system model and

simulation, while Section 5 reports the results and analysis. The study concludes in section 6 with an overall summary and discussion of the findings.

## 2. Kinematics Modeling of Robot

Kinematic modeling in robotics creates a mathematical model of a robot's motion, excluding the forces that caused that motion. The model is typically used to describe the planning (trajectory) of the End-Effector of the WidowX 250 robot as it moves through space, such as the gripper at the arm's End-Effector. A robot's kinematic model is typically split into two parts: Forward Kinematic and Inverse Kinematic [22]. The FK describes the correlation between the position, orientation, and joint angles of the WidowX-250 robot EE. The FK can be implemented to find the orientation and position of the EE in 3D space given the joint angles. Meanwhile, the IK is applied to obtain the joint angles to achieve the desired EE orientation and position. It was frequently used in motion planning and control applications where the robot must move to a specific location or manipulate an object in a specific manner [23].

### 2.1. Mechanism of Robotic Arm

A manipulator, also known as a robotic arm, is a mechanical system implemented to mimic the movement of a human arm. It was typically made up of a number of rigid links (segments) connected by joints (actuators) that allow the arm to move in various directions. Consequently, the revolute joint is the most common type in robot arms, allowing rotation around a single axis. Meanwhile, prismatic and spherical joints allow linear motion along a single axis and rotation around multiple axes, respectively [24]. Moreover, actuators are important parts of the robot system, such as electric motors or hydraulic cylinders, which control the arm's movement. Thus, actuators apply torque or force to the joints to move the arm through its various degrees of freedom. Furthermore, Sensors such as encoders or potentiometers are used to measure the position and velocity of each joint, and this information is fed back to a controller, which computes the necessary actuator commands to achieve the desired arm movement.

The end-effector is attached to the last link of the robotic arm, which is usually a tool or gripper. The end-effector performs various tasks and can be programmed to manipulate objects, pick up, weld, drill, and paint. A mechanism of the robotic arm is manufactured to visualize its performance for multiple tasks. The factors of the robotic arm, such as payload, capacity, the range of motion, speed, and precision of the arm, are all considered when designing and manufacturing it. The control system and the advancements in the science of materials have resulted in the development of robot arms capable of performing multiple tasks with higher efficiency and accuracy [25]. Table 1 shows the properties of the WidowX 250 6DOF manipulator. Default joint limits are the safe range of operation for each joint, as shown in Table 2. Fig. 1 shows the WidowX 250 6DOF arm links [26]. Table 3 illustrates the Links and length (mm) of WidowX 250 6DOF [26].

**Table 1.** Properties of WidowX 250 6DOF Manipulator [26].

WidowX-250 6DOF	
Degrees of Freedom	6
Reach	650mm
Total span	1300mm
Accuracy	1mm
Working Payload	250g
Total Servos	9
Wrist Rotate	Yes

**Table 2.** Default Joint Limits [26].

Joint	Min	Max	ServoID(s)
Waist	-180	180	1
Shoulder	-108	114	2+3
Elbow	-123	92	4+5
Wrist Angle	-100	123	6
Forearm Roll	-180	180	7
Wrist Rotate	-180	180	8
Gripper	30mm	74mm	9

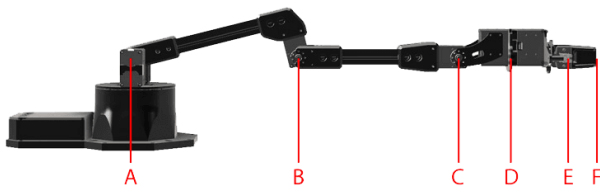


**Figure 1.** WidowX 250 arm links [26].

**Table 3.** Links and length (mm) of WidowX 250 6DOF [26].

Link A	Link B	Link C	Link D	Link E	Link F
Arm Base	Elbow Joint	Wrist Tilt Joint	Wrist Rotate	Gripper Rail	Finger Tip

**2.2. WidowX 250 Robot Arm**

WidowX 250 6DOF robotic arm can move in six directions. It is manufactured by Trossen Robotics with a high-performance arm and was built for education and research. The WidowX 250 robotic arm has six degrees of freedom, meaning it can perform precise multi-movements. It has a reach of up to forty-one cm and can carry up to 0.25 kg of payload. WidowX 250 is the most powerful robotic arm in the X series family of robotic manipulators. The X series family has more effective heat dissipation in a small form factor than previous robot versions and has current, actuators, and torque that offer strong action with high durability. The main purpose of using the WidowX 250 robotic arm is the highest efficiency, besides its raised maneuverability. Moreover, the pose of an arm can be described using the orientation (pitch, roll, and yaw) and position (x, y, and z) of its end effector in 3D space. While each of these factors of the pose of the arm must be constrained by lower DOF arms, one or more of them can be controlled independently with a six-degree-of-freedom arm. Also, the

WidowX 250 has a modular design that allows users to remove or add components to tailor the arm to their specific requirements. It has many options and accessories, such as wrist rotation, grippers, and custom end-effectors. Overall, the WidowX 250 robotic arms are a complex system that combines electronic and mechanical components to provide robust and precise movement. Its customizable control options and modular design make it an adaptable tool for various applications [27], [28].

**2.3. Denavit Hartenberg DH Convention**

The forward kinematics problems deal with the relationship between the orientation and position of the end-effector or the tool and the individual joints of the robot manipulator. As described in the previous section, a manipulator of robots comprises links connected by various joints. The joints are divided into simple (such as a prismatic joint or a revolute joint) and complex (such as a socket and a ball joint). The Denavit-Hartenberg (DH) matrices have four quantities  $a_i, \alpha_i, d_i, \theta_i$ , which are generally associated with link  $i$  and joint  $i$ , given the names link length, twist angle, link offset, and joint angle, respectively [29]. Denavit and Hartenberg developed the symbolic notation that completely describes lower pair mechanisms. This symbolic notation furnishes a reliable analytical procedure and a robust approach since the operations depend on matrix algebra. These parameters are the revolute joint  $\theta_i$  or joint variable, and three quantities would be fixed parameters of the link. The definition of manipulator through these parameters is conventionally called Denavit-Hartenberg notation [29].

Forward kinematics may be computed directly from a product of the exponentials of the POE chain. The POE method uses only two frames of reference: the tool frame T and the base frame S. In order to reduce six parameters to four for Denavit-Hartenberg twists parameters, the Denavit-Hartenberg parameters for a robot require the careful selection of the tool frame to enable cancellations. In the product of the exponential method, the joint twists are easier to construct directly without considering adjacent joints in the chain and are easier to process by computer. Moreover, prismatic and revolute joints are treated separately and uniformly using DH parameters in the POE method. The equations below depict the kinematic properties (product of exponentials) for the WidowX 250 6DOF robotic arm [30]-[33].

$$g_{st}(0) = \begin{bmatrix} R & p \\ 0 & 1 \end{bmatrix} \tag{1}$$

$$M = \begin{bmatrix} 1.0 & 0.0 & 0.0 & 0.458325 \\ 0.0 & 1.0 & 0.0 & 0.0 \\ 0.0 & 0.0 & 1.0 & 0.36065 \\ 0.0 & 0.0 & 0.0 & 1.0 \end{bmatrix} \tag{2}$$

$S_{list} =$

$$\begin{bmatrix} 0.0 & 0.0 & 1.0 & 0.0 & 0.0 & 0.0 \\ 0.0 & 1.0 & 0.0 & -0.11065 & 0.0 & 0.0 \\ 0.0 & 1.0 & 0.0 & -0.36065 & 0.0 & 0.04975 \\ 1.0 & 0.0 & 0.0 & 0.0 & 0.36065 & 0.0 \\ 0.0 & 1.0 & 0.0 & -0.36065 & 0.0 & 0.29975 \\ 1.0 & 0.0 & 0.0 & 0.0 & 0.36065 & 0.0 \end{bmatrix}^T \quad (3)$$

Where:  $g_{st}$  is the transformation matrix from the tool frame to the base frame,  $R$  is the rotation matrix,  $p$  is the translation vector,  $M$  is the Position and Orientation of the End Effector matrix, and  $S_{list}$  is the Spatial twist matrix.

**3. Methods**

Some considerations, including software and hardware, must be highlighted to ensure that the robot moves correctly. As a result, the software should be simple to use and stable to avoid problems. Moreover, hardware is important in implementing a solid robot that will move as planned. The algorithm in this study was created using MATLAB software (MathWorks) and ROS (Robot Operating System).

**3.1. Forward and Inverse Kinematic Analysis**

FK analysis is utilized to find the orientation and position of the EE given the joint angles. In contrast, IK analysis determines the joint angles needed to position the EE at a particular orientation and position. The DH convention technique was utilized for forward modeling. The CFS approach was utilized to find all sets of probable solutions for IK modeling. Following that, a correlation analysis was performed to see if there was any relationship between the FK and IK models. Finally, performance was assessed using waypoint-tracking and trajectory-planning algorithms in ROS and MATLAB [24]-[28].

**3.2. Modeling of Forward Kinematics**

The DH convention technique for modeling the FK of the robot is composed of three stages. The first stage involves analyzing the robot arm's configuration to determine its DH parameters. Fig. 2 depicts the dimensions analysis in mm for the WidowX 250 Robotic arm. Table 4 displays the D-H convention parameters for the WidowX 250 robotic arm obtained after the configured analysis. Fig. 3 shows the WidowX 250 Robotic arm model with all six degrees of freedom and links [28].

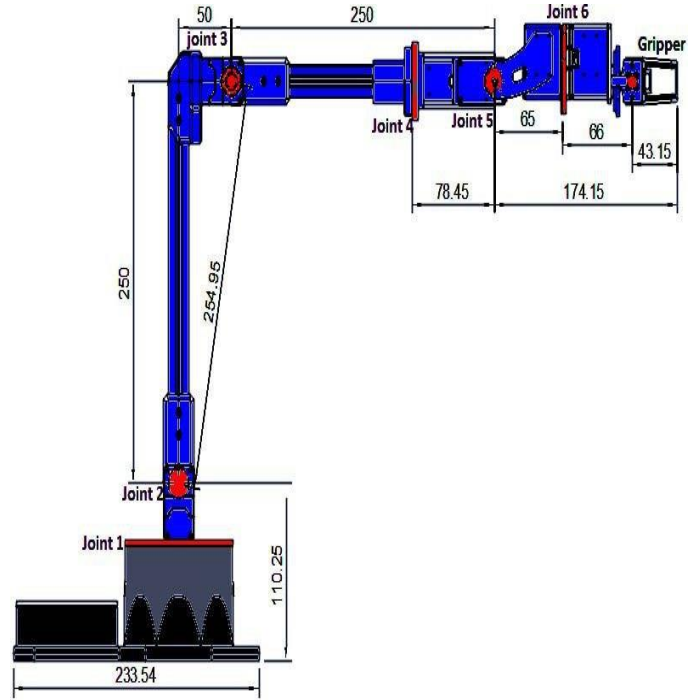


**Figure 2.** WidowX 250 robotic arm dimensions analysis in mm [28].

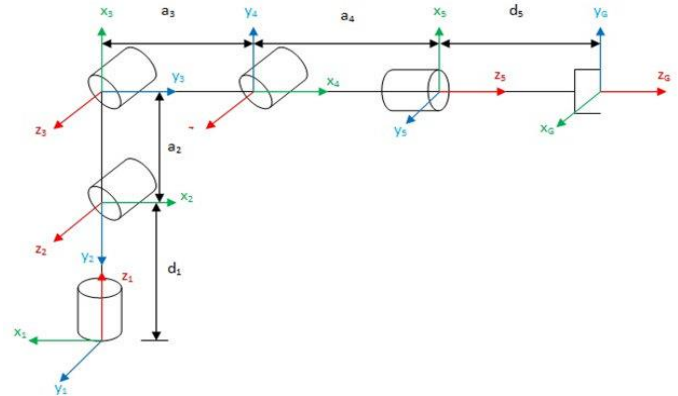


**Figure 3.** WidowX 250 robotic arm model with all six degrees of freedom and links [28].

On the robot arm configuration, there is a displacement between joints 2 and 3, resulting in an offset angle. The offset angle is defined and taken into account in the DH parameters. There are nine servos, one for the gripper and eight for the arm. According to the schematic, servos two and four are on the robot's back, while servos three and five are on the Front. To provide the required torque, Joints two and three each have two servos: For joint two, servo three rotates in the same direction as  $\theta_2$ , whereas servo two is the complement, i.e.,  $180-\theta_2$ . For joint three, servo five rotates in the same direction as  $\theta_3$ , while servo four is its complement, i.e.,  $180-\theta_5$ . Servo seven rotates in the same direction as  $\theta_5$ . The transformation matrix is calculated using the DH convention in the next stage.

The DH parameters will be included in the transformation matrix after they have been determined. Because 6 DOFs were used, the linked matrix's limit is  $T_6^0$ . Fig. 4 illustrates the

computation of the offset angle  $\theta_0$  between Joints 2,3 for the WidowX 250 robotic arm [28]-[32].

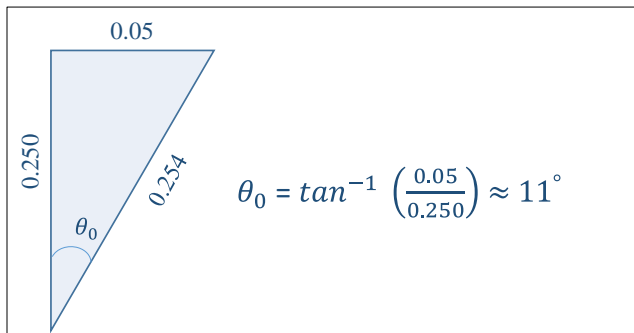


**Figure 4.** The computation of the offset Angle,  $\theta_0$ , between Joints 2,3 [28].

The transformation matrix equations are as follows [33]-[35]:

$$T_1^0 = \begin{bmatrix} \cos(\theta_1) & 0 & -\sin(\theta_1) & 0 \\ \sin(\theta_1) & 0 & \cos(\theta_1) & 0 \\ 0 & -1 & 0 & d_1 \\ 0 & 0 & 0 & 1 \end{bmatrix} \quad (4)$$

$$T_2^1 = \begin{bmatrix} -\sin(\theta_0 + \theta_2) & \cos(\theta_0 + \theta_2) & 0 & -a_2 * \sin(\theta_0 + \theta_2) \\ \cos(\theta_0 + \theta_2) & -\sin(\theta_0 + \theta_2) & 0 & a_2 * \cos(\theta_0 + \theta_2) \\ 0 & 0 & 1 & 0 \\ 0 & 0 & 0 & 1 \end{bmatrix} \quad (5)$$

$$T_3^2 = \begin{bmatrix} \cos(\theta_0 - \theta_3) & 0 & -\sin(\theta_0 - \theta_3) & 0 \\ -\sin(\theta_0 - \theta_3) & 0 & -\cos(\theta_0 - \theta_3) & 0 \\ 0 & 1 & 0 & 0 \\ 0 & 0 & 0 & 1 \end{bmatrix} \quad (6)$$

$$T_4^3 = \begin{bmatrix} \cos(\theta_4) & 0 & -\sin(\theta_4) & 0 \\ \sin(\theta_4) & 0 & \cos(\theta_4) & 0 \\ 0 & -1 & 0 & d_4 \\ 0 & 0 & 0 & 1 \end{bmatrix} \quad (7)$$

$$T_5^4 = \begin{bmatrix} \cos(\theta_5) & 0 & \sin(\theta_5) & 0 \\ \sin(\theta_5) & 0 & -\cos(\theta_5) & 0 \\ 0 & 1 & 0 & 0 \\ 0 & 0 & 0 & 1 \end{bmatrix} \quad (8)$$

$$T_6^5 = \begin{bmatrix} \cos(\theta_6) & 0 & -\sin(\theta_6) & 0 \\ \sin(\theta_6) & 0 & \cos(\theta_6) & 0 \\ 0 & -1 & 0 & d_6 \\ 0 & 0 & 0 & 1 \end{bmatrix} \quad (9)$$

The next step is combining the values of  $T_1^0$ ,  $T_2^1$ ,  $T_3^2$ ,  $T_4^3$ ,  $T_5^4$ , and  $T_6^5$  in sequence and clarifying them.

$$T_6^0 = T_1^0 \cdot T_2^1 \cdot T_3^2 \cdot T_4^3 \cdot T_5^4 \cdot T_6^5 \quad (10)$$

The final stage is obtaining the position vector for the EE. After simplification, the equation of the transformation matrix is as follows:

$$T_6^0 = \begin{bmatrix} n_x & o_x & a_x & p_x \\ n_y & o_y & a_y & p_y \\ n_z & o_z & a_z & p_z \\ 0 & 0 & 0 & 1 \end{bmatrix} \quad (11)$$

Where  $n$  ( $n_x, n_y, n_z$ ),  $o$  ( $o_x, o_y, o_z$ ), and  $a$  ( $a_x, a_y, a_z$ ) are orthogonal unit vectors that define the orientation of the frame for the EE as decelerated in the following:

$$n_x = c_1 c_2 s_3 s_4 s_6 - c_5 c_6 s_1 s_4 - c_1 c_2 c_3 c_6 s_5 - c_4 s_1 s_6 + c_1 c_3 s_2 s_4 s_6 + c_1 c_6 s_2 s_3 s_5 - c_1 c_2 c_4 c_5 c_6 s_3 - c_1 c_3 c_4 c_5 c_6 s_2 \quad (12)$$

$$o_x = s_1 s_4 s_5 - c_1 c_2 c_3 c_5 + c_1 c_5 s_2 s_3 + c_1 c_2 c_4 s_3 s_5 + c_1 c_3 c_4 s_2 s_5 \quad (13)$$

$$a_x = c_5 s_1 s_4 s_6 - c_4 c_6 s_1 + c_1 c_2 c_6 s_3 s_4 + c_1 c_3 c_6 s_2 s_4 + c_1 c_2 c_3 s_5 s_6 - c_1 s_2 s_3 s_5 s_6 + c_1 c_2 c_4 c_5 s_3 s_6 + c_1 c_3 c_4 c_5 s_2 s_6 \quad (14)$$

$$n_y = c_1 c_4 s_6 + c_1 c_5 c_6 s_4 - c_2 c_3 c_6 s_1 s_5 + c_2 s_1 s_3 s_4 s_6 + c_3 s_1 s_2 s_4 s_6 + c_6 s_1 s_2 s_3 s_5 - c_2 c_4 c_5 c_6 s_1 s_3 - c_3 c_4 c_5 c_6 s_1 s_2 \quad (15)$$

$$o_y = c_5 s_1 s_2 s_3 - c_2 c_3 c_5 s_1 - c_1 s_4 s_5 + c_2 c_4 s_1 s_3 s_5 + c_3 c_4 s_1 s_2 s_5 \quad (16)$$

$$a_y = c_1 c_4 c_6 - c_1 c_5 s_4 s_6 + c_2 c_6 s_1 s_3 s_4 + c_3 c_6 s_1 s_2 s_4 + c_2 c_3 s_1 s_5 s_6 - s_1 s_2 s_3 s_5 s_6 + c_2 c_4 c_5 s_1 s_3 s_6 + c_3 c_4 c_5 s_1 s_2 s_6 \quad (17)$$

$$n_z = c_2 c_3 s_4 s_6 + c_2 c_6 s_3 s_5 + c_3 c_6 s_2 s_5 - s_2 s_3 s_4 s_6 - c_2 c_3 c_4 c_5 c_6 + c_4 c_5 c_6 s_2 s_3 \quad (18)$$

$$o_z = c_2 c_5 s_3 + c_3 c_5 s_2 + c_2 c_3 c_4 s_5 + c_4 s_2 s_3 s_5 \quad (19)$$

$$a_z = c_2 c_3 c_6 s_4 - c_6 s_2 s_3 s_4 - c_2 s_3 s_5 s_6 - c_2 s_2 s_5 s_6 + c_2 c_3 c_4 c_5 s_6 - c_4 c_5 s_2 s_3 s_6 \quad (20)$$

where (c) relates to cos and (s) to sin. While the p ( $p_x, p_y, p_z$ ) is the position vector of the EE as decelerated in the following equations:

$$p_x = d_4 c_1 c_2 c_3 - a_2 c_0 c_1 s_2 - a_2 c_1 c_2 s_0 - d_4 c_1 s_2 s_3 - d_6 s_1 s_4 s_5 + d_6 c_1 c_2 c_3 c_5 - d_6 c_1 c_5 s_2 s_3 - d_6 c_1 c_2 c_4 s_3 s_5 - d_6 c_1 c_3 c_4 s_2 s_5 \quad (21)$$

$$p_y = d_4 c_2 c_3 s_1 - a_2 c_0 s_1 s_2 - a_2 c_2 s_0 s_1 + d_6 c_1 s_4 s_5 - d_4 s_1 s_2 s_3 + d_6 c_2 c_3 c_5 s_1 - d_6 c_5 s_1 s_2 s_3 - d_6 c_2 c_4 s_1 s_3 s_5 - d_6 c_3 c_4 s_1 s_2 s_5 \quad (22)$$

$$p_z = d_1 - d_4 c_2 s_3 - d_4 c_2 s_3 - d_4 c_3 s_2 + a_2 s_0 s_2 - d_6 c_2 c_5 s_3 - d_6 c_3 c_5 s_2 - d_6 c_2 c_3 c_4 s_5 + d_6 c_4 s_2 s_3 s_5 \quad (23)$$

### 3.3. Modeling of Inverse Kinematics

The IK equations for a 6-DOF robotic arm such as the WidowX 250 can be complex. However, in general, they involve solving a set of nonlinear equations that relate the joint positions and orientations to the desired EE position and orientation. Fig. 5 shows the Widow X250 robotic arm joints with assigned angles [36].

**Table 4.** Link DH parameters table of widowX250 6DOF robot arm [28]-[30].

Link <sub><i>i</i></sub>	<i>a<sub>i</sub></i> (m)	<i>α<sub>i</sub></i> (deg)	<i>d<sub>i</sub></i> (m)	<i>θ<sub>i</sub></i> (deg)	range <i>θ<sub>i</sub></i> (deg.)
1	0	-90	0.11025	<i>θ<sub>1</sub></i>	-180 to 180
2	-0.25495	0	0	<i>θ<sub>2</sub></i> +90 +11.5	-108 to 114
3	0	90	0	<i>θ<sub>3</sub></i> -11.5	-123 to 92
4	0	-90	0.25	<i>θ<sub>4</sub></i>	-100 to 123
5	0	90	0	<i>θ<sub>5</sub></i>	-180 to 180
6	0	0	0.157625	<i>θ<sub>6</sub></i>	-180 to 180

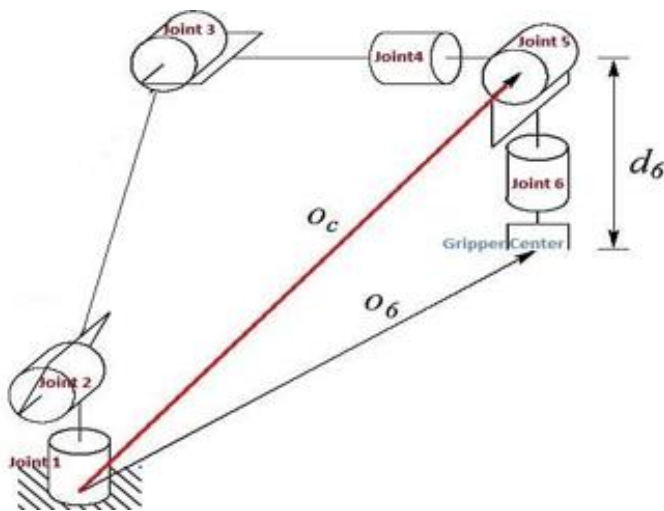


**Figure 5.** The joints of the robotic arm [26].

*θ<sub>1</sub>*, *θ<sub>2</sub>*, and *θ<sub>3</sub>* can be calculated using the following:

$$\theta_1 = \text{Atan2}(p_x; p_y) \tag{24}$$

$$\theta_2 = \text{Atan2}(\sqrt{p_x^2 + p_y^2 - d^2}; p_z - d_1) - \text{Atan2}(a_2 + a_3c_3; a_3s_3) \tag{25}$$

$$\theta_3 = \text{Atan2}(D; \pm\sqrt{1 + D^2}) \tag{26}$$

Where D is:

$$D = \frac{p_x^2 + p_y^2 - d^2 + (p_z - d_1)^2 - a_2^2 - a_3^2}{2a_2a_3} \tag{27}$$

while *θ<sub>4</sub>*, *θ<sub>5</sub>*, and *θ<sub>6</sub>* calculated using the following equations

$$\theta_4 = \text{Atan2}(s_1o_x - c_1o_y; c_1s_{23}o_x + s_1s_{23}o_y + c_{23}o_z) \tag{28}$$

$$\theta_5 = \text{Atan2}(\pm\sqrt{1 - (-c_1c_{23}o_x - s_1c_{23}o_y; + s_{23}o_z)^2} - c_1c_{23}o_x - s_1c_{23}o_y; + s_{23}o_z) \tag{29}$$

$$\theta_6 = \text{Atan2}(c_1c_{23}a_x + s_1c_{23}a_y - s_{23}a_z; -c_1c_{23}n_x + s_1c_{23}n_y + s_{23}n_z) \tag{30}$$

## 4. Results and Discussion

In this section, the results of MATLAB modeling are provided and compared to the findings obtained by ROS for the position of the end-effector arm in FK. In addition, the angle values in modeling IK are derived from the position values in FK.

### 4.1. Forward Kinematics Modeling

Table 4 illustrates the results of the EE-coordinate using MATLAB. Ten cases have been taken in this study to obtain the joint variables in (rad) and the EE-Coordinate (*p<sub>x</sub>*, *p<sub>y</sub>*, *p<sub>z</sub>*) in (mm). The angle values from *θ<sub>1</sub>* to *θ<sub>6</sub>* have been assumed, and *p<sub>x</sub>*, *p<sub>y</sub>*, and *p<sub>z</sub>* were

obtained using (21), (22), and (23). Table 5 also demonstrates the results of EE coordination using ROS, using 10 similar states that were applied in MATLAB to construct variables and the EE Coordinates.

Table 6 shows the error of EE-Coordinates between Tables 2 and 3, which means the error between MATLAB and ROS in calculating *p<sub>x</sub>*, *p<sub>y</sub>*, and *p<sub>z</sub>* values, and the most significant margin of errors appeared in case 3 in *p<sub>y</sub>* and case 7 in *p<sub>x</sub>*. Table 6 shows the error of EE-Coordinates between MATLAB and ROS in calculating *p<sub>x</sub>*, *p<sub>y</sub>*, and *p<sub>z</sub>* values. The flowchart of the forward kinematic modeling approach is shown in Fig. 6. The created algorithm contains D-H parameters to get the end-effector's coordinates of the robotic arm, and the transformation matrix is computed to obtain the equations for the end-effector's coordinates. Fig. 7 and Fig. 8 present a sample of the End-Effector Coordinates simulation results for the set of solutions for the position using MATLAB and RO, S, respectively. In these modeling, two different positions have been considered, the first end effector coordinate was (*p<sub>x</sub>* = 0.458, *p<sub>y</sub>* = 0.000, *p<sub>z</sub>* = 0.360), Which illustrates the first case (home position), and the second was (*p<sub>x</sub>* = 0.262, *p<sub>y</sub>* = 0.184, *p<sub>z</sub>* = 0.056), That indicates the fourth case. The two used programs (MATLAB and ROS) showed virtually the same outcome. Also, case 1 (left image of Fig. 7) was set at (90.0° Roll, -0.0° Pitch, and -90.0° Yaw). Thus, case 4 (right image of Fig. 7) was set at (-179.7° Roll, 24.8° Pitch, and -75.1° Yaw).

Table 7 shows the accuracy between MATLAB and ROS of the EE coordinates.

In case 1 (below image of Fig. 8), ROS was set the position at (0.407; 0; 0.361) and the orientation at (0; 0.00077; 0;1) for arm link and position at (0.458; 0; 0.361) and the orientation at (0;

0.00077; 0;1) for gripper link. In case 4 (above image of Fig. 8), ROS was set the position at (0.2622; 0.1707; -0.0) and the orientation at (0.241; 0.704; -0.05;0.6) for arm link and position at (0.2622; 0.183; -0.05) and the orientation at (0.241; 0.704; -0.05;0.6641) for gripper link.

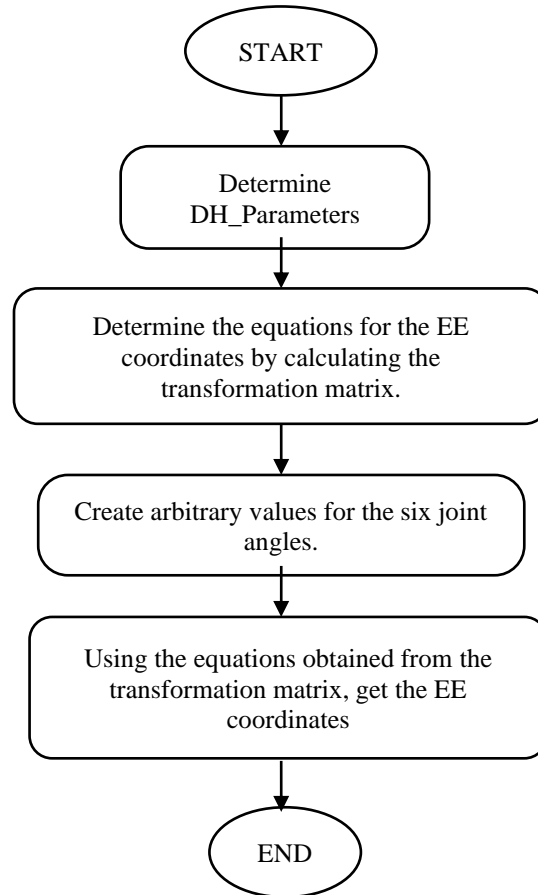


Figure 6. Forward kinematic modeling algorithm flowchart.

Table 5. ROS results of EE coordinates.

Case	Joint Variable (rad)						EE_Coordinates (m)		
	$\theta_1$	$\theta_2$	$\theta_3$	$\theta_4$	$\theta_5$	$\theta_6$	$P_x$	$P_y$	$P_z$
1	0	0	0	0	0	0	0.45824	0	0.361272
2	1	1	1	1	1	1	-0.0779	0.086538	-0.07016
3	-1	-1	-1	-1	-1	-1	-0.11482	0.390145	0.561395
4	0.5	0.5	0.5	0.5	0.5	0.5	0.262225	0.183944	-0.05605
5	-0.5	-0.5	-0.5	-0.5	-0.5	-0.5	0.089376	-0.00805	0.716458
6	1.5	1.5	1.5	1.5	1.5	1.5	-0.15789	0.004146	0.053919
7	-1.5	-1.5	-1.5	-1.5	-1.5	-1.5	0.124107	0.515107	0.203323
8	0	0	0.95	0	2.15	1.32	0.036126	0.0005	0.150201
9	0	-1.57	1.61	0	0.48	1.44	0.137752	0	0.073497
10	0	-1.57	1.61	0	0	1.44	0.158274	0	0.146393

**Table 6.** Error between MATLAB and ROS of the EE coordinates.

Case	Error (mm)		
	$P_x$	$P_y$	$P_z$
1	0.06	0	1.172
2	1.8021	1.5221	2.155
3	0.676	3.745	1.405
4	0.325	0.456	1.2991
5	2.9659	2.13306	0.058
6	0.894	0.31483	2.3593
7	3.407	0.493	0.977
8	2.4543	0.001	0.001
9	0.952	0	0.7166
10	0.774	0	1.593

**Table 7.** The accuracy between MATLAB and ROS of the EE coordinates.

Case	Accuracy (%)		
	$P_x$	$P_y$	$P_z$
1	99.994	100	99.8828
2	99.81979	99.84779	99.7845
3	99.9324	99.6255	99.8595
4	99.9675	99.9544	99.87009
5	99.70341	99.78669	99.9942
6	99.9106	99.96852	99.76407
7	99.6593	99.9507	99.9023
8	99.75457	99.9999	99.9999
9	99.9048	100	99.92834
10	99.9226	100	99.8407

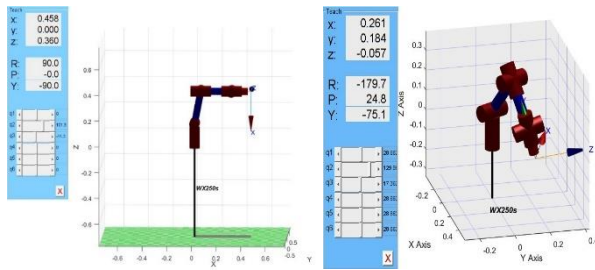


**Figure 7.** Modeling through MATLAB End-Effector Coordinates' results. Act Case 1 for the left image and Act Case 4 for the right image.

Fig. 9 shows the EE-frame ( $p_x$ ,  $p_y$ , and  $p_z$ ) derived by ROS simulation and MATLAB modeling and their comparison for the ten imposed scenarios, which show that they are similar and equivalent.

Fig. 10 depicts the accuracy between the two comparative sections and for every case, with the lowest accuracy being 99.6% and the maximum accuracy being 100%.

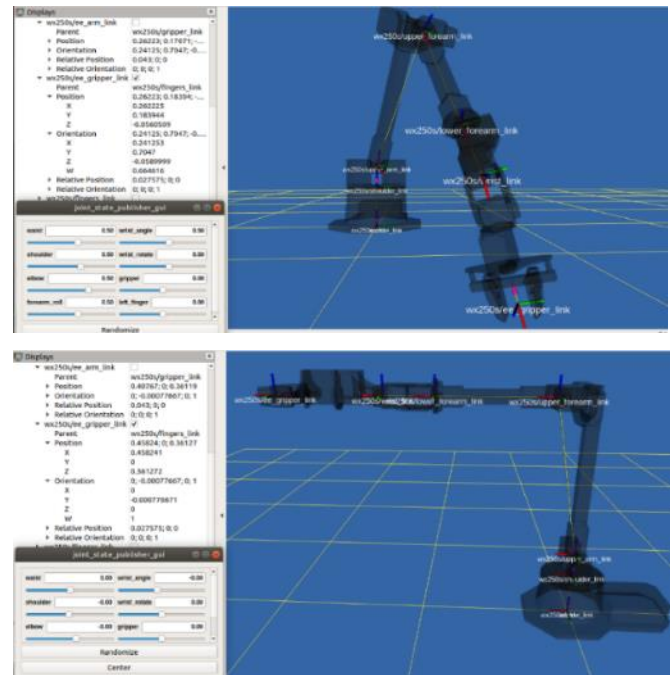


**Figure 8.** ROS simulation results of End-Effector coordinates. Act Case 1 is for the image below, while Act Case 4 is for the image above.

#### 4.2. Inverse Kinematics Modeling

Table 8 presents the findings of IK modeling, showing a set of solutions for joint angles in rad for ten situations. The joint angle solutions for the IK model are presented in Table 5. There are ten cases to verify the inverse kinematics. (24) to (30) were used to determine the IK of the robotic arm. It produced various results, some of which were close to expectations, while others were far away from them. As is well known, one of the most significant features of IK modeling is difficulty in deriving and achieving the same results as FK modeling, especially if the arm has more than 3DOF. As a result, numerical techniques, optimization, and artificial intelligence technologies are used to handle such challenges. An interesting observation is that the angle of the third joint remains constant between  $\pm 1.57$  radians across all instances studied, indicating certain limitations in the arm's motion range. From equation 26 (for  $\theta_3$ ), it remains constant between  $\pm 90^\circ$  and according to the end-effector. Also, the arm is redundant. While  $\theta_1$  ranged from  $0^\circ$  to  $180^\circ$ , it was significantly higher in case 9. Meanwhile, the  $\theta_6$  of the arm ranges from  $(28.7^\circ$  to  $122.7^\circ)$  (30). The flowchart of the inverse kinematic modeling algorithm is shown in Fig. 11. The end-effector coordinates are sent into the algorithm to determine the joint angles required for achieving the desired end-effector position.

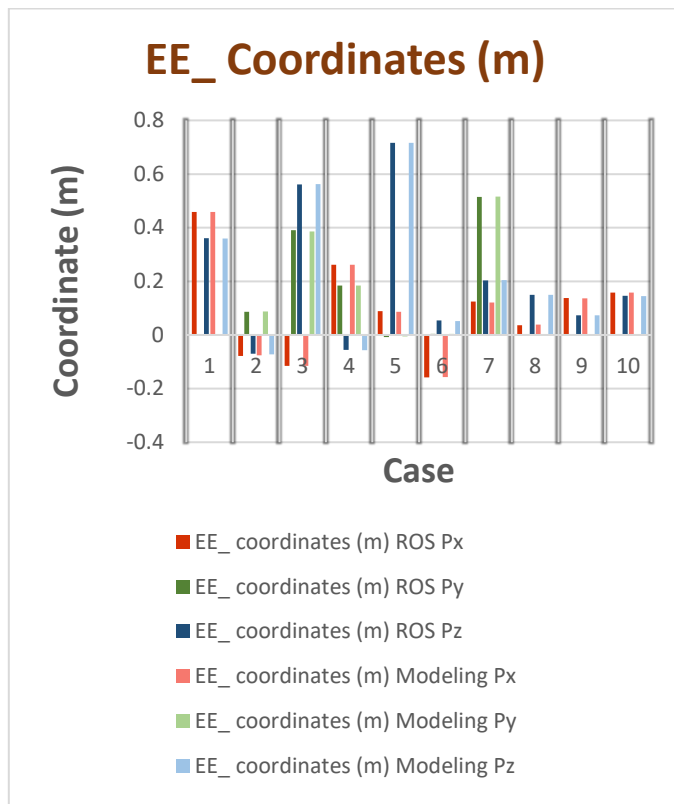


Figure 9. ROS via MATLAB modeling EE-coordinates.

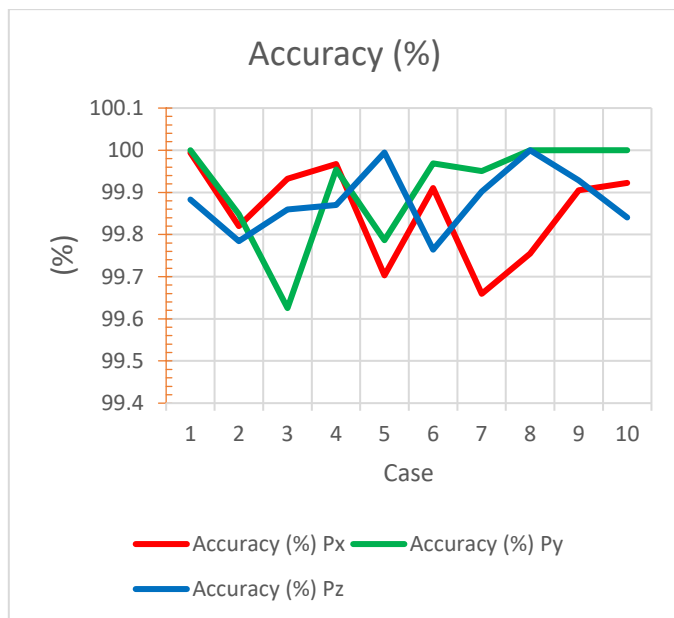


Figure 10. ROS via MATLAB EE-Coordinates accuracy.

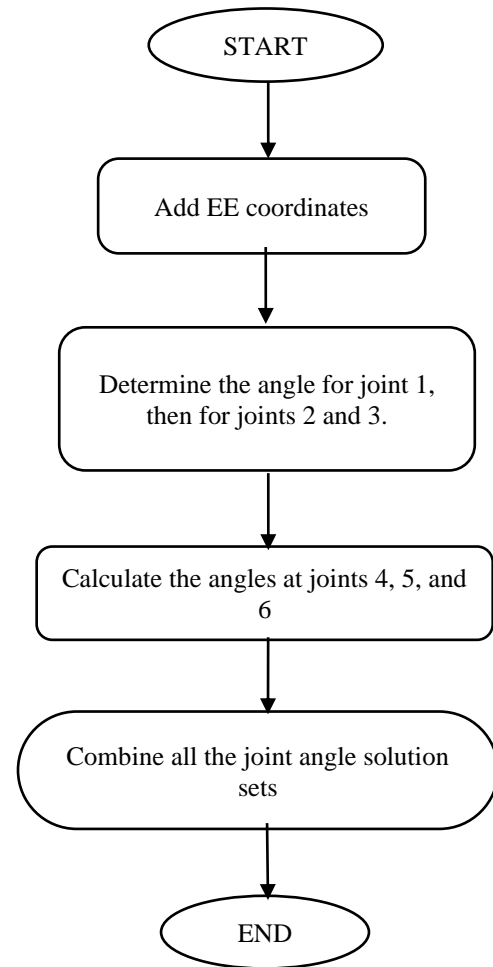


Figure 11. Inverse kinematic modeling algorithm flowchart

**5. Conclusions**

Based on this investigation, the forward and inverse kinematics modeling for the WidowX250-6DOF robotic arm, manufactured by Interbotix, was successfully executed. This work could significantly impact various applications, including industrial automation, healthcare, and even entertainment. The FK and IK of the Widowx250 6DOF have been derived and implemented. The results obtained for the FK of the arm, conducted through MATLAB modeling, and compared with the ROS simulation results, showed a matching percentage of over 99% for the end effector position and the arm in general. However, for the IK,

the results revealed a range of solutions for each joint angle, some of which were close to the desired results, and others were not. The value of the third joint angle was established at  $\pm 1.57$  radians, requiring further future studies to refine the results using various numerical analysis methods such as fuzzy logic, artificial intelligence, and modern robotics techniques. Also, future work will test the optimized model based on a theoretical foundation in areas such as path planning, kinematic optimization, and structural design for robots.

**Table 8.** Inverse kinematic modeling results.

Case	$\theta_1(\text{rad})$	$\theta_2(\text{rad})$	$\theta_3(\text{rad})$	$\theta_4(\text{rad})$	$\theta_5(\text{rad})$	$\theta_6(\text{rad})$
1	0.0000	-2.7561	1.5708	-1.5708	3.1416	1.5708
	3.1416	3.5271	-1.5708	1.5708	-3.1416	-1.5708
2	1.0000	-0.3855	1.5708	1.0000	1.0000	1.0000
	4.1416	5.8977	-1.5708	-2.1416	-1.0000	-2.1416
3	2.1416	-3.9318	1.5708	2.1416	1.0000	2.1416
	5.2832	2.3514	-1.5708	-1.0000	-1.0000	-1.0000
4	0.5000	-5.4930	1.5708	0.5000	0.5000	0.5000
	3.6416	0.7902	-1.5708	-2.6416	-0.5000	-2.6416
5	-0.5000	-1.7016	1.5708	2.6416	0.5000	2.6416
	2.6416	4.5816	-1.5708	-0.5000	-0.5000	-0.5000
6	1.5000	4.8432	1.5708	1.5000	1.5000	1.5000
	4.6416	-4.6336	-1.5708	-1.6416	-1.5000	-1.6416
7	1.6416	1.4921	1.5708	1.6416	1.5000	1.6416
	4.7832	-2.9348	-1.5708	-1.5000	-1.5000	-1.5000
8	0.0000	3.3484	1.5708	0.0000	2.1500	1.3200
	3.1416	-0.2068	-1.5708	-3.1416	-2.1500	-1.8216
9	3.1416	6.0764	1.5708	0.0000	0.4800	1.4400
	6.2832	-1.5727	-1.5708	-3.1416	-0.4800	-1.7016
10	3.1416	4.7105	1.5708	1.5708	0.0000	1.6952
	6.2832	-1.5727	-1.5708	-1.5708	-0.0000	-1.4464

**Acknowledgements**

The authors thank the College of Engineering- University of Wasit for using the WidowX 250 6 DOF robotic arm and supporting this work.

**Abbreviations**

- $g_{st}$  transformation matrix from the tool frame to the base frame
- $M$  the Position and Orientation of the End Effector matrix
- $p$  the translation vector,
- $p$  base

- $R$  the rotation matrix
- $S_{list}$  the Spatial twist matrix.
- $\theta$  direction, (rad)

**Nomenclature**

- CFS Closed-form solutions
- DOF Degree of Freedom
- EE End-Effector
- IK Inverse Kinematic
- FK Forward Kinematic
- ROS Robot Operating System

## Conflict of interest

The authors declare no conflict of interest.

## Author Contribution Statement

Hasan A. Obied proposed the research problem.

Hasan A. Obied and Manaf K. H. Al-Taleb developed the theory and performed the computations.

Hind Zuhair Khaleel and Ali F. AbdulKareem verified the analytical methods and supervised the findings of this work.

All authors discussed the results and contributed to the final manuscript.

## Data Availability

Not applicable.

## References

- [1] W. I. M. Al-Tameemi and W. M. H. Hadi, "Kinematics analysis of 5250 lab-volt 5-DOF robot arm," *Eng. Tech. J.*, vol. 32, no. 1, pp. 2196–2204, 2014, <https://doi.org/10.30684/etj.32.9A8>.
- [2] P. Corke, W. Jachimczyk, and R. Pillat, "Robot manipulators," in *Robotics, Vision and Control*, 3rd ed., vol. 147, Springer Tracts in Advanced Robotics. Switzerland: Springer, 2023, pp. 275–327.
- [3] J. Ondras et al., "Robotic dough shaping," in *2022 22nd Int. Conf. Control, Autom. Syst. (ICCAS)*, Jeju, Korea, 2022, <https://doi.org/10.48550/arXiv.2208.00386>.
- [4] K. M. Lynch and F. C. Park, "Grasping and manipulation," in *Modern Robotics: Mechanics, Planning, and Control*, 1st ed. Cambridge, UK: Cambridge Univ. Press, 2017, pp. 396–433.
- [5] H. Z. Ting et al., "Kinematic analysis for trajectory planning of open-source 4-DOF robot arm," *Int. J. Adv. Comput. Sci. Appl.*, vol. 12, no. 6, pp. 769–777, 2021, <https://doi.org/10.14569/IJACSA.2021.0120690>.
- [6] G. Singh and V. K. Banga, "Robots and its types for industrial applications," *Mater. Today Proc.*, vol. 60, pt. 3, pp. 1779–1786, <https://doi.org/10.1016/j.matpr.2021.12.426>.
- [7] G. Bao, S. Liu, and H. Zhao, "Kinematics simulation of 4 DOF manipulator," in *MSMEE*, vol. 123, 2017, pp. 400–408.
- [8] Z. Chao et al., "Inverse kinematics solution and verification of 4-DOF hydraulic manipulator," *J. Phys.: Conf. Ser.*, vol. 916, pp. 1–8. DOI <https://iopscience.iop.org/article/10.1088/1742-6596/916/1/012022>
- [9] T. Dewi et al., "Inverse kinematic analysis of 4 DOF pick and place arm robot manipulator using fuzzy logic controller," *Int. J. Electr. Comput. Eng.*, vol. 10, no. 2, pp. 1376–1386, 2020, <https://doi.org/10.11591/ijece.v10i2.ppl1376-1386>.
- [10] S. Gómez et al., "Design of a 4-DOF robot manipulator with optimized algorithm for inverse kinematics," *Int. J. Mech. Mechatronics Eng.*, vol. 9, no. 6, pp. 929–934, 2015, <https://doi.org/10.5281/zenodo.1105267>.
- [11] A. Singh and A. Singla, "Kinematic modeling of robotic manipulators," *Proc. Natl. Acad. Sci. India Sect. A Phys. Sci.*, vol. 87, pp. 303–319, 2017, <https://doi.org/10.1007/s40010-016-0285-x>.
- [12] S. F. F. Shero et al., "Assessment of linear parameters of electrohysterograph (EHG) in diagnosis of true labor," *Ann. Trop. Med. Public Health*, vol. 23, no. 4, pp. 139–147, 2020, <https://doi.org/10.36295/ASRO.2020.23418>.
- [13] F. A. Raheem and H. Z. Khaleel, "Robot arm design for children writing ability enhancement using Cartesian equations based on ANFIS," in *2018 Third Sci. Conf. Electr. Eng. (SCEE)*, 2018, pp. 150–155, <https://doi.org/10.1109/SCEE.2018.8684038>.
- [14] S. Das and S. S. Mahapatra, "Prediction of inverse kinematics of a 5-DOF pioneer robotic arm having 6-DOF end-effector using ANFIS," *Int. J. Comput. Vis. Robot.*, vol. 5, no. 4, pp. 365–384, 2015, <https://doi.org/10.1504/IJCVR.2015.072190>.
- [15] H. A. R. Akkar and A. Najim A-Amir, "Kinematics analysis and modeling of 6 degree of freedom robotic arm from DFROBOT on Labview," *Res. J. Appl. Sci. Eng. Technol.*, vol. 13, no. 7, pp. 569–575, 2016, <https://doi.org/10.19026/rjaset.13.3016>.
- [16] H. Z. Khaleel, "Inverse kinematics solution for redundant robot manipulator using combination of GA and NN," *Al-Khwarizmi Eng. J.*, vol. 14, no. 1, pp. 136–144, 2018, <https://doi.org/10.22153/kej.2018.10.008>.
- [17] J. I.-Z. Chen and J.-T. Chang, "Applying a 6-axis mechanical arm combine with computer vision to the research of object recognition in plane inspection," *J. Artif. Intell. Capsul. Networks*, vol. 2, no. 2, pp. 77–99, 2020, <https://doi.org/10.36548/jaicn.2020.2.002>.
- [18] K. S. Gaeid et al., "Robot control and kinematic analysis with 6DoF manipulator using direct kinematic method," *Bull. Electr. Eng. Inform.*, vol. 10, no. 1, pp. 70–78, 2021, <https://doi.org/10.11591/eei.v10i1.2482>.
- [19] H. Chih-Ching et al., "Kinematic analysis of a 6-DOF robotic arm," *Springer Int. Publ.*, vol. 73, no. 16, pp. 2965–2974, 2019, [https://doi.org/10.1007/978-3-030-20131-9\\_292](https://doi.org/10.1007/978-3-030-20131-9_292).
- [20] S. Luo et al., "Inverse kinematics solution of 6-DOF manipulator based on optimization PSO algorithm," *Front. Neurobot.*, vol. 16, Mar. 2022, <https://doi.org/10.3389/fnbot.2022.791796>.
- [21] H. A. Obied, M. H. Kadhum, and A. F. AbdulKareem, "Visualizing kinematics: Investigating the impact of altered joint angles on end-effector position and orientation using Rviz and WidowX250-6DOF," *Wasit J. Eng. Sci.*, vol. 12, no. 2, pp. 1–14, 2024, <https://doi.org/10.31185/ejuow.Vol12.Iss2.477>.
- [22] A. A. Mohammed and M. Sunar, "Kinematics modeling of a 4-DOF robotic arm," in *2015 Int. Conf. Control, Autom. Robot. (ICCAR)*, 2015, pp. 87–91, <https://doi.org/10.1109/ICCAR.2015.7166008>.
- [23] T. O. Terefe et al., "Kinematic modeling and analysis of a walking machine (robot) leg mechanism on a rough terrain," *Adv. Sci. Technol. Res. J.*, vol. 13, no. 3, pp. 43–53, 2019, <https://doi.org/10.12913/22998624/109792>.
- [24] H.-S. Kim and J.-B. Song, "Multi-DOF counterbalance mechanism for a service robot arm," *IEEE/ASME Trans. Mechatronics*, vol. 19, no. 6, pp. 1756–1763, 2014, <https://doi.org/10.1109/TMECH.2014.2308312>.
- [25] J. Cai et al., "Modeling method of autonomous robot manipulator based on DH algorithm," *Mobile Inf. Syst.*, vol. 2021, pp. 1–10, 2021, <https://doi.org/10.1155/2021/4448648>.
- [26] Trossen Robotics, "WIDOWX 250 robot arm," *X-Series Robotic Arm*, 2022. [Online]. Available: <https://www.trossenrobotics.com/widowx-250-robot-arm.aspx> (Accessed: Jul. 12, 2023).
- [27] Z. Fu, X. Cheng, and D. Pathak, "Deep whole-body control: Learning a unified policy for manipulation and locomotion," in *Conf. Robot Learn.*, 2023, pp. 138–149, <https://doi.org/10.48550/arXiv.2210.10044>.
- [28] RoboSavvy, "Trossen Robotis WidowX 250 Robot Arm (6DOF)." [Online]. Available: <https://robosavvy.co.uk/trossen-robotis-widowx-250-robot-arm-6dof-m.html> (Accessed: Jun. 6, 2024).
- [29] P. I. Corke, "A simple and systematic approach to assigning Denavit–Hartenberg parameters," *IEEE Trans. Robot.*, vol. 23, no. 3, pp. 590–594, 2007, <https://doi.org/10.1109/TRO.2007.896765>.
- [30] A. C. Reddy, "Difference between Denavit–Hartenberg (DH) classical and modified conventions for forward kinematics of robots with case study," in *Int. Conf. Adv. Mater. Manuf. Technol. (AMMT)*, 2015, pp. 267–286, <https://doi.org/10.13140/2.1.2012.9607>.
- [31] M. van Hoeij, "Closed form solutions for linear differential and difference equation," in *Proc. 2017 ACM Int. Symp. Symbolic Algebraic Comput.*, 2017, pp. 3–4, <https://doi.org/10.1145/3087604.3087660>.

- [32] M. W. Spong, S. Hutchinson, and M. Vidyasagar, "Forward and inverse kinematics," in *Robot Modeling and Control*, 2nd ed. New York: Wiley, 2006, pp. 73–117.
- [33] C. W. Wampler, "Manipulator inverse kinematic solutions based on vector formulations and damped least-squares methods," *IEEE Trans. Syst., Man, Cybern.*, vol. 16, no. 1, pp. 93–101, 1986, <https://doi.org/10.1109/TSMC.1986.289285>.
- [34] P. Agnihotri, V. K. Banga, and E. G. Singh, "Review of kinematic modelling and control of 5 degree of freedom robotic arm using DH representation," *Int. J. Electr. Electron. Eng.*, vol. 7, no. 2, pp. 140–148, 2015.
- [35] P. Lin, W. Y. Choi, and C. C. Chung, "Local path planning using artificial potential field for waypoint tracking with collision avoidance," in *2020 IEEE 23rd Int. Conf. Intell. Transp. Syst. (ITSC)*, 2020, pp. 1–7, <https://doi.org/10.1109/ITSC45102.2020.9294717>.
- [36] T. Davies and A. Jnifene, "Multiple waypoint path planning for a mobile robot using genetic algorithms," in *2006 IEEE Int. Conf. Comput. Intell. Meas. Syst. Appl.*, 2006, pp. 21–26, <https://doi.org/10.1109/CIMSA.2006.250741>.